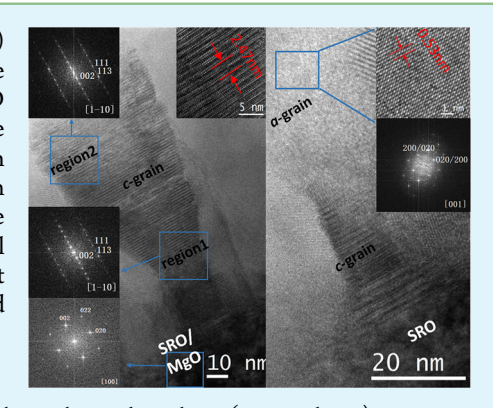


Strain Engineered CaBi₂Nb₂O₉ Thin Films with Enhanced Electrical **Properties**

Yunxiang Zhang,^{†,‡} Jun Ouyang,^{*,†,‡,⊥} Jincan Zhang,^{†,‡} Yao Li,^{†,‡} Hongbo Cheng,^{†,‡} Huiwen Xu,^{†,‡} Menglin Liu,^{†,‡} Zhao-Peng Cao,[†] and Chun-Ming Wang^{*,†}

Supporting Information

ABSTRACT: In this work, strain engineered polycrystalline thin films (~250 nm) of bismuth layer-structured ferroelectric (BLSF) CaBi₂Nb₂O₉ (CBNO) were prepared by using a radio frequency (RF) magnetron sputtering technique. XRD analysis revealed that the films were (200)/(020) and (00l) textured with a large in-plane tensile stress. Cross-sectional TEM analyses confirmed the bismuth layered-structure, as well as crystalline orientations and a strain-controlled growth mode of the grains. Result of a quantitative XPS analysis revealed that the composition of the film is close to the chemical stoichiometry. Excellent electrical properties were achieved in the CBNO films, including a high dielectric constant (~280 @5 kHz), a small dielectric loss ($tg\delta \le 1.6\%$ up to an applied electric field of ~1200 kV/cm) and a large polarization ($P_r \approx 14 \,\mu\text{C/cm}^2 \, @ 1 \,\text{kHz}$).



KEYWORDS: strain engineering, bismuth layer-structured ferroelectrics (BLSFs), calcium bismuth niobate (CaBi₂Nb₂O₉), magnetron sputtering, electrical property

1. INTRODUCTION

Since 1949, when Aurivillius discovered bismuth layerstructured ferroelectrics (BLSFs), this type of ferroelectric has attracted significant amount of research interest because of to their unique features, such as a high fatigue resistance, a low aging rate, as well as a good temperature stability of properties endowed by a high Curie temperature $(T_c)^{2-5}$ These features are desirable for the development of ferroelectric-based electrical devices working under severe conditions. FeRAM for military mobile electronics and high-temperature piezoelectrics are two examples of such devices.4-6 However, with large anisotropies in the ion displacements, the spontaneous polarization of a BLSF mainly exists in the a-b plane and is generally quite small along the c axis. ^{2,7} Unlike the pseudocubic perovskite ceramics whose polarizations can be easily reoriented under an applied electric field, BLSFs' unique layered structure ($a \approx b \ll c$) makes it difficult to realign their crystallites with different orientations. Therefore, the electrical displacement and electromechanical responses are usually small for a BLSF ceramic.³⁻

Calcium bismuth niobate (CaBi₂Nb₂O₉, or CBNO), which consists of alternative $(CaNb_2O_7)^{2^-}$ and $(Bi_2O_2)^{2^+}$ layers in its lattice, is a member of the BLSFs. ⁸⁻¹² It has a very high Curie temperature ($T_c \approx 943$ °C), one of the highest in its family and among all ferroelectrics. After the early works by I. G. Ismailzade¹³ and S.M. Blake, ¹⁴ H. X. Yan et al. reported for the first time a systematic study on preparation of textured and randomly oriented CBNO ceramics via spark plasma sintering (SPS) and ordinary firing techniques, respectively.8 The measured remnant polarization (Pr) was $\sim 7.5 \mu \text{C/cm}^2$ for the textured ceramic and $\sim 2.5 \,\mu\text{C/cm}^2$ for a random one, both being small as compared with the theoretical value (\sim 24.4 μ C/ cm²).⁸ This indicates that there's still plenty of room for property enhancement. Later on, electrical properties of CBNO ceramics, especially dielectric and piezoelectric properties, were intensively investigated by several groups. 9-12,15-21 Most of the reported work focused on modification of the unit cell of CBNO via doping or substitution, which have led to substantial yet not decisive property enhancements. For example, the reported dielectric constants and piezoelectric moduli are more or less in the same range as those of undoped CBNO ceramics. The relative dielectric constants $\varepsilon_{\rm r}$ are between 80 and 100 while the piezoelectric moduli d_{33} are between 10 and 20 pm/

Growth of oriented films, while meeting the ever-increasing demand of device miniaturization and integration, provides a

Received: January 9, 2016 Accepted: June 13, 2016 Published: June 13, 2016



[†]Key Laboratory for Liquid–Solid Structural Evolution and Processing of Materials (Ministry of Education), School of Materials Science and Engineering and School of Physics, State Key Laboratory of Crystal Materials, Shandong University, Jinan, Shandong 250061, China

FSuzhou Institute of Shandong University, Suzhou 215123, China

 $^{^{\}perp}$ National Institute of Standards and Technology, Gaithersburg, Maryland 20899, United States

solution for the enhancement of electrical properties of ferroelectrics. Cho and Desu^{22,23} and A. Z. Simões et al. A-27 are the two major groups who reported preparations of CBNO thin films and investigated their electrical properties. The former fabricated highly c-axis oriented CBNO films with a remnant polarization ~3.6 μ C/cm² using a pulsed laser deposition method, 22,23 while the latter prepared highly a-and c-axis oriented thin films with a remnant polarization ~4.2 μ C/cm² via a polymer precursor method. Their results confirmed that with an increasing amount of a-axis oriented grains (a-grains), that is, the (200)/(020) crystallites, ferroelectric and piezoelectric properties of a CBNO film showed a clear trend of improvement. Recently, Y. Ahn et al. prepared epitaxial c-axis oriented (c-grain) and highly a-axis oriented CBNO thin films via pulsed laser deposition. The remnant polarizations of their films were improved to ~10 μ C/cm².

Despite these significant improvements on the properties of CBNO films, there have been very few investigations focusing on enhancing their electrical performance via strain engineering, which has been broadly adopted in the design and preparation of perovskite ferroelectric thin films. This method utilizes the misfit strain imposed by an underlying substrate or a buffer layer to select grain orientation of a polycrystalline film, 30,31 or to enhance electrical properties of a single-domain epitaxial film. Moreover, this method can also be used to design domain architectures in a polydomain epitaxial film. In this work, the effectiveness of strain engineering for textured growth and property enhancement of a CBNO thin film is demonstrated.

Commonly used substrates for epitaxial or highly textured growth of BLSFs are single crystalline perovskite oxide substrates including NdGaO₃, SrTiO₃, LaAlO₃ etc.^{34,35} Such a substrate has a lattice parameter either well matched with the a/b-axis of a BLSF like CBNO ($a \approx 5.5 \text{ Å} \approx a_{CBNO}$) (Figure 1a), or matched with the diagonal of the BLSF's (00l)-plane (a $\approx 3.8-4 \text{ Å} \approx a_{\text{CBNO}}/\sqrt{2})$ (Figure 1b), both leading to a (100)//(001) heteroepitaxy. In either case, a conductive perovskite oxide like SrRuO₃ ($a_{SRO} \approx 4$ Å), can be used as the bottom electrode layer preserving the aforementioned heteroepitaxy (Figure 1c).36 However, BLSF films grown on such substrates are c-axis oriented, which have shown small ferroelectric polarizations and unimpressive electromechanical properties. To obtain a high quality a-axis oriented film of BLSF, a complex thin film heterostructure including a special buffer layer is required. ^{2,29} In our study, CBNO thin films were sputtered on unbuffered, single crystalline MgO substrates with a lattice parameter of 4.2 Å. The MgO substrate was chosen not only for its excellent properties (low dielectric loss, for example³⁷) and cost-effectiveness as compared to complex oxide substrates, but also for an increased lattice mismatch with the c-grain of a CBNO film. The computed lattice mismatches (unrelaxed misfit strains) are listed in Table 1. Since the a, baxis of CBNO showed about twice as large lattice mismatch with $[101]_{MgO}$, as compared to that between the c-axis and $[4\overline{0}4]_{MgO}$, it is expected that abundant a-grains and grains tilting away from the c-axis can be created in the CBNO films grown on MgO at the expense of the c-grains. In addition, the in-plane stress will be predominantly tensile (for both a- and cgains), which can significantly enhance longitudinal electromechanical properties of a ferroelectric film (dielectric constant $\varepsilon_{\rm r}$ and piezo modulus d_{33}), as have been reported by Li and Nagarajan et al. on thin films of barium strontium titanate and lead magnesium niobate-lead titanate. 32,40,41

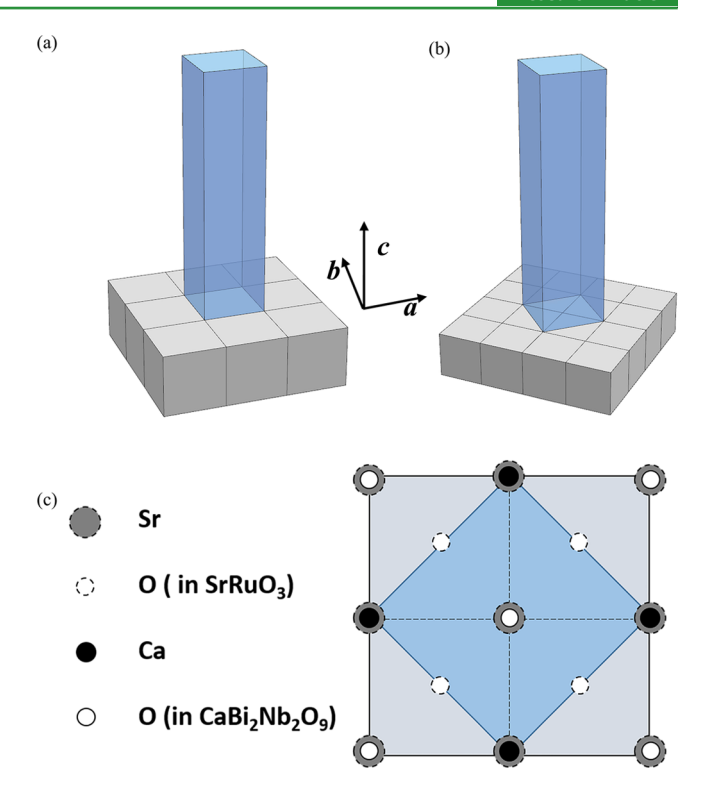


Figure 1. Illustration of lattice matching between a *c*-axis oriented CBNO grain (*c*-grain) and a perovskite oxide substrate with (a) $a \approx 5.5 \text{ Å}$; (b) $a \approx 4 \text{ Å}$; (c) a perovskite bottom electrode layer of SrRuO₃, $a_{\text{CBNO}}/\sqrt{2} \approx a_{\text{SRO}} < \sim 4 \text{ Å}$; where a, a_{CBNO} , and a_{SRO} are the substrate lattice parameter, a-axis lattice parameter of CBNO and lattice parameter of SrRuO₃, respectively.

Table 1. Lattice Constants of Relevant Materials and Their Mismatches

materials	CBNO ceramic ^{10,26}	MgO (100)	SrRuO ₃ and CBNO film on MgO
lattice constants (nm)	a = 0.5435 b = 0.5466	$\sqrt{2a} = 0.5957$	SRO, $\sqrt{2}a = 0.5629$ CBNO, $a = b = 0.5260$ (agrain)
	c = 2.4970	$4\sqrt{2}a = 2.3829$	$c = 2.465 \ (c-grain)$
lattice mismatch with MgO at room temperature $(\%)^{SS}$		a-axis = 8.78 b-axis = 8.26 c-axis = -4.77	
thermal expansion coefficients $(\times 10^{-6}/\mathrm{K})$ between room temperature and growth temperature		a/b-axis = -2.5 c -axis = 12^{38}	
lattice mismatch with MgO at growth temperature (%)		a-axis = 9.63 b-axis = 9.11 c-aixs = -4.68	
out-of-plane film strain (%)		a-axis = $-3.22b$ -axis = $-3.77c$ -axis = -1.27	

^aExtrapolated to growth temperature.

2. EXPERIMENTAL SECTION

A cylinder shape (Φ = 50 mm, t = 5 mm) CaBi₂Nb₂O₉ target was calcined at 1120 °C for 10 h using a reactive sintering method and annealed at 700 °C in air for 6 h to stabilize its structure and properties. The starting materials were CaCO₃ (99.9% purity), Bi₂O₃ (99.9%), and Nb₂O₅ (99.5%), with molar ratios determined by the stoichiometric ratios of metal ions in CaBi₂Nb₂O₉, except that 5% mol excessive bismuth oxide was added to compensate its evaporation loss.

The CBNO films were sputtered on single crystalline (100) MgO substrates in a vacuum chamber with a base pressure of 2.5×10^{-4} Pa at 600 °C. Prior to the film growth, a conductive oxide bottom electrode of SrRuO3 was deposited under similar conditions as the CBNO film. Details of the sputtering process were summarized in Table 2. It is noted that to minimize deviation from the stoichiometry

Table 2. Deposition Parameters of the Sputtering Process

sputtering parameters	$SrRuO_3$	CaBi ₂ Nb ₂ O ₉	
thickness (nm)	50	250	
substrate temperature (°C)	600		
sputtering power (W)	70		
deposition atmosphere	$Ar:O_2 = 32:8 \text{ (sccm)}$		
deposition pressure (Pa)	1.2		
cooling atmosphere	$Ar:O_2 = 32:8 \text{ (sccm)}$		
holding time (min)	10		
heating/cooling rate (°C/min)	6-8		
target-substrate distance (mm)	50		

of CaBi₂Nb₂O₉, we chose a moderate sputtering power and an optimal sputtering atmosphere with an Ar/O₂ flow ratio of 4:1. While the former limits the bulk diffusion of the target and hence help maintain its self-compensating mechanism of stoichiometry in a preferential sputtering process, 42 the latter has been proven to yield sputtered peroskite films with both a dense microstructure and a good chemical stoichiometry.43,44

The phase structure and crystallographic orientations of the films were analyzed by using X-ray θ -2 θ scans (via a commercial Rigaku Dmax-rc XRD diffractometer equipped with a Ni-filtered Cu-Kα radiation source) and pole figures (via a Rigaku SmartLab XRD, R-Axis Spider, 40 kV, 200 mA). Transmission electron microscopy (TEM, via a JEOL JEM-2100HR) was used to investigate nanostructures of the film. Chemical composition and valence states of the elements were analyzed via X-ray photoelectron spectroscopy (XPS) using an ESCALAB 220i-XL electron spectrometer (VG Scientific) equipped with a 300W Al K α radiation source. Roomtemperature pseudostatic ferroelectric hysteresis loops were measured by using a Radiant Precision Premier II ferroelectric tester, while the dielectric properties (C-V characteristics) of the films were obtained by using an impedance analyzer (HP4194A, Hewlett-Packard Ltd.). Prior to the electrical characterizations, circular Au top electrodes (Φ = 200 μ m) were sputtered at room temperature via a shadow mask.

3. RESULTS AND DISCUSSION

XRD 2θ scan spectrum of the CBNO film is shown in Figure 2, which was indexed according to refs 8 and 12. The CBNO film showed a polycrystalline structure with main diffraction peaks located at (200)/(020), (00l) (l = 4, 6, 8, 10, 14), (111), and (119). It is noted that the (200) and (020) diffraction peaks could not be distinguished from each other due to the similar

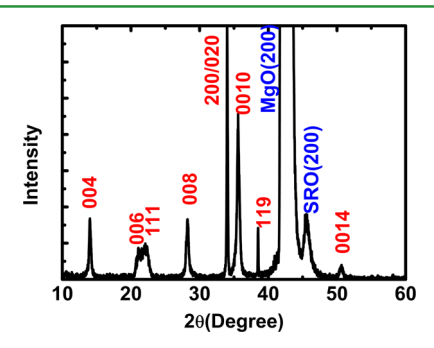
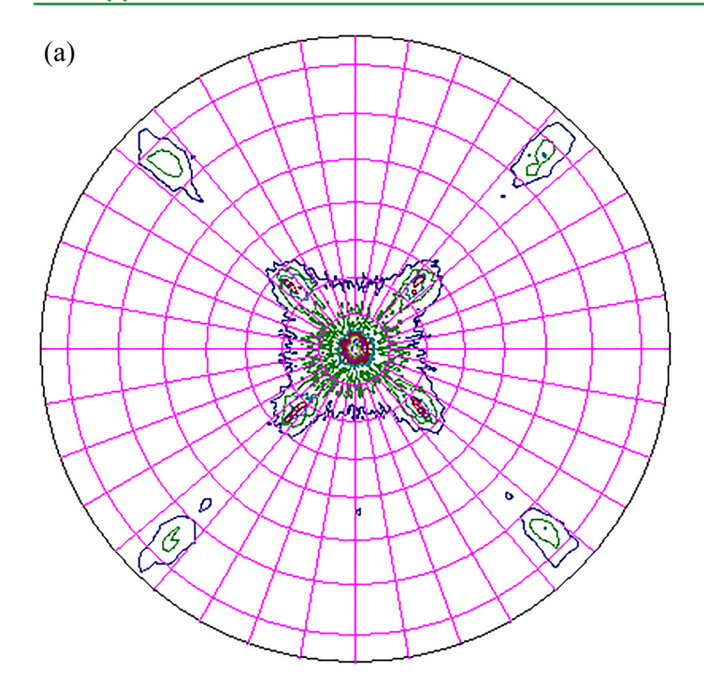


Figure 2. XRD 2θ scan spectrum of the CBNO films sputtered on $SrRuO_3/(100)MgO$.

lattice parameters of a- and b-axis. From the XRD pattern, the lattice parameters of a/b-axis and c-axis were computed and listed in Table 1. These out-of-plane lattice parameters were slightly smaller (1-3%) than those of the CBNO ceramics, indicating a dominant tensile residual stress in the growth plane (along the in-plane a/b axis). This residual stress is a collective result of multiple sources of misfit strains, including an initial lattice misfit and a postgrowth thermal strain, which was developed during cooling down of the thin film heterostructure. From the XRD data, it can be concluded that we have successfully prepared a tensile strained CBNO film with substantial amount of a-grains.

To further investigate the film's texture, X-ray pole figures were recorded by using the (200)/(020) and (0010) reflection peaks and are shown in Figure 3a and b, respectively. During the measurement, the samples were rotated by varying the tilt angle $(0^{\circ} < \psi < 70^{\circ})$ and the azimuthal angle $(0^{\circ} < \phi < 360^{\circ})$ with respect to the scattering vector. The (200)/(020) pole figure consists of three distinct sets of peaks. The central diffraction spot surrounding $\psi = 0$ came from the {200} grains (a-grains), which shows the maximum diffraction intensity. This indicates that the films are highly a-axis textured. The 4fold diffraction peaks at $\psi \approx 26^{\circ}$ correspond to the {315} plane, and another set of 4-fold diffraction peaks at $\psi \approx 65^{\circ}$ correspond to the {119} plane. The X-ray diffractions were concentrated in the tilt angles between $\psi = 0^{\circ}$ and $\psi = 30^{\circ}$, suggesting a sizable remnant polarization with contributions from not only the a-grains, but also grains slightly tilting away from the main polarization axis. On the other hand, the (0010) pole figure shows a very strong and sharp central diffraction spot together with a set of 4-fold diffraction peaks at $\psi \approx 57^{\circ}$ which corresponds to the $\{103\}$ plane. Together with the 2θ scan results, the pole figure analyses indicate that the c-grains are epitaxially grown on the (100) MgO substrate with a mixture of other grains, including textured a-grains and those tilting away from the main axis.

Nanostructures of the CBNO films were analyzed via TEM and the representative results are shown in Figure 4. Figure 4a is a cross-sectional bright field TEM image of the film, which showed periodically aligned nanosized *c*-grains (numbered from 1 to 10 in the figure). These columnar grains grew across the whole film thickness with an increasing lateral radius (from \sim 20 nm near the bottom electrode to \sim 50-70 nm near the film surface). The growth mode of the c-grains can be clearly observed in Figure 4b. Near the bottom electrode where a cgrain started an epitaxial growth due to a good lattice matching with SrRuO₃ (as shown in Figure 1a), elastic energy dominated and restricted its lateral expansion. As the film thickness was increased, the misfit strain was relaxed and hence the c-grain grew with an increasing lateral radius. Moreover, a layeredstructure of the CBNO film is clearly observed in Figure 4b. The average (002) spacing, or the c-axis lattice parameter, can be directly measured from the high-resolution TEM image (inset of Figure 4b), which is about 2.47 nm and consistent with the XRD data. The in-plane growth geometry of the cgrain was revealed by the attached FFT patterns, which is $\lfloor 110 \rfloor_{CBNO} / / \lfloor 010 \rfloor_{SRO/MgO,}$ and consistent with the literature (Figure 1). Furthermore, the average lattice parameters computed from the line scan of several unit cells were compared to validate the strain-controlled growth mode. Region 2 far away from the bottom electrode showed ~0.8% increase of the c-axis lattice parameter as compared with that of region 1, the neck region of the up-side down bottle-shaped c-



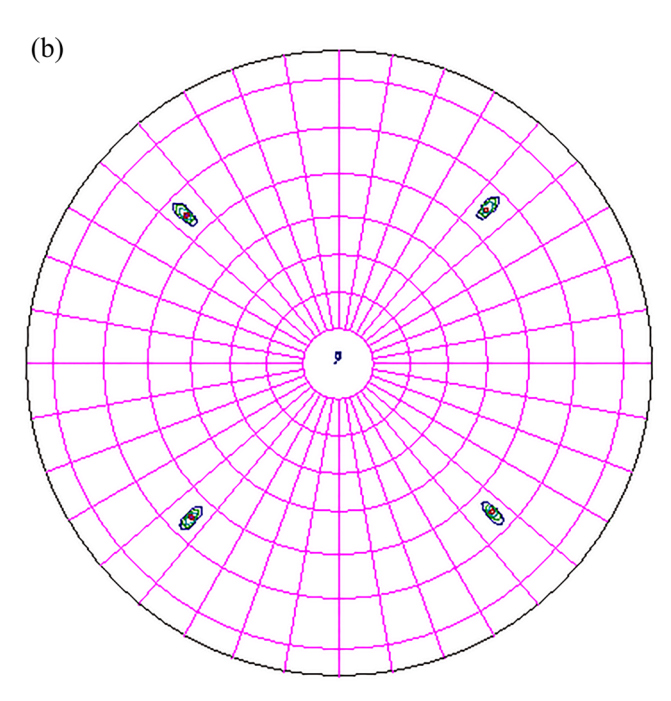


Figure 3. X-ray pole figure analyses by using the (a) (200)/(020) and (b) (0010) reflections of the CBNO film.

grain where the stress is concentrated. This corresponds to a reduction of the in-plane tensile strain by ~1.2% in the fully grown part of the c-grain (assuming Poisson ratio $\sim 1/3$). On the other hand, a typical cross-sectional TEM image of an agrain is shown in Figure 4(c), which grew from the side of a neighboring c-grain instead of the interface with the bottom electrode, owing to its poor lattice matching with the SRO electrode layer. Moreover, an a-axis lattice parameter of \sim 0.53 nm was measured from the high resolution TEM image, which is also consistent with the XRD data and supports our design of a tensile-strained CBNO film.

XPS analysis was carried out to estimate chemical composition of the film and investigate valence states of the

elements. The base pressure in the sample chamber of the XPS spectrometer was 3×10^{-9} mbar and no Ar⁺ etching was used prior to the collection of photoelectrons to avoid reduction of the oxides. 45,46 Figure 5a is the XPS spectrum of the original surface of CBNO film in the energy range between 0 and 600 eV. It clearly shows the existence of Ca, Bi, Nb and O in their corresponding valence states in CBNO (Ca²⁺, Bi³⁺, Nb⁵⁺ and O²⁻). It should be noted that, except for some adventitious C which is used for calibration of the binding energies (C 1s line at 284.8 eV), there is no clear signature of other elements, or different valence states of the cations. The trace of carbon comes from two possible sources, carbon in the air and surface carbon contamination during sample preparation for XPS. EDS spectrum obtained for the bulk of the film showed no detectable amount of carbon, indicating that carbon only exists as surface contaminant. Since the electrical properties were measured from top electrode-covered CBNO capacitors, effects of surface carbon contaminant on the electrical properties were

The film's composition near the surface was estimated to be n_{Ca} : n_{Bi} : n_{Nb} : $n_{\text{O}} \approx 0.9$:1.8:2.4:9.6 via quantitative analysis of Figure 5a, which is close to the stoichiometric ratio of the elements. Furthermore, photoemissions of Ca 2p, Bi 4f, and Nb 3d core levels were performed, and the results are shown in Figure 5b-d, respectively. In Figure 5b, the binding energies of Ca $2p_{3/2}$ and Ca $2p_{1/2}$ are revealed to be 346.8 and 350.9 eV, respectively, matching those of the Ca-O bond in CaO. This indicates that the Ca element exists in the form of Ca²⁺ in the CBNO film. Similarly, the binding energies of Bi $4f_{7/2}$ and Bi $4f_{5/2}$ (159.0 and 164.3 eV, respectively, as shown in Figure 5c) and of Nb $3d_{5/2}$ and Nb $3d_{3/2}$ (206.7 and 209.51 eV, respectively, as shown in Figure 5d), are all consistent with those reported in literature for the valence states of $Bi^{3+25,45,46} and \ Nb^{5+.25,45}$

Figure 6 showed the voltage dependent dielectric constant $(\varepsilon_r - V)$ and loss tangent $(tg\delta - V)$ of the CBNO film measured at 5 kHz. The ε_r -V curve exhibited a typical butterfly shape, indicating a sound ferroelectricity which manifested itself via domain switching. The maximum value of the dielectric constant (~283) appears near the zero field, a nearly 100% improvement against the best reported values (~140-150) in the literature. ²⁵ A sizable dielectric tunability $\eta = [1 - \varepsilon_r(E_{max})/$ $\varepsilon_{\rm r}(0)$] × 100% = 47% was achieved in the CBNO thin film, where $\varepsilon_{\rm r}(0) = 283$ and $\varepsilon_{\rm r}(E_{\rm max}) = 150$ are the dielectric constants at zero field and the maximum bias field $E_{\text{max}} = 1200$ kV/cm, respectively. Furthermore, the dielectric loss tangent ${\rm tg}\delta$ is <~1.6% at $E_{\rm max}$ resulting in a superior figure of merit (FOM) for the dielectric tunability, FOM = tunability/loss tangent ~30, significantly higher than those of the CBNO films reported in the literature (FOM $\sim 10-15$). ^{26,27} The greatly enhanced dielectric properties can be understood by the combination of the two effects from strain engineering. First, the strained growth of the film on the chosen substrate of MgO results in reduction of c-grains, which were replaced by a-grains and grains tilting away from the a/b axis, leading to a better average polarization and a larger dielectric constant, as evidenced by the pioneering work on textured CBNO ceramics.⁸ Second, according to the work by Li and Nagarajan et al. on dielectric properties of stressed ferroelectric films, 32,40,41 an in-plane tensile stress can further improve the longitudinal dielectric response. This is the case for our CBNO films.

ACS Applied Materials & Interfaces

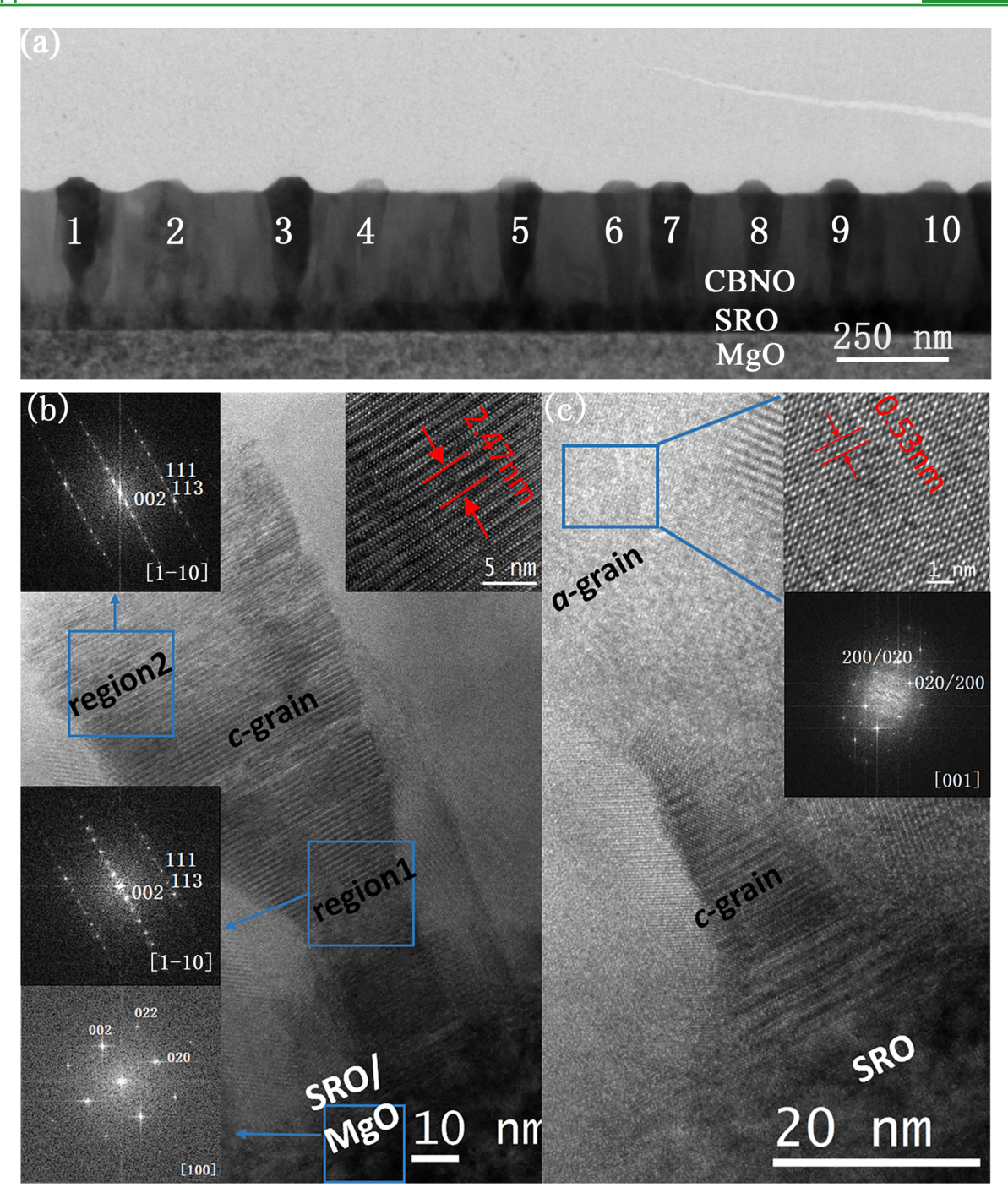


Figure 4. (a) Cross-sectional bright field TEM image of the CBNO thin film heterostructure with c-grains being marked from "1" to "10", and typical cross-sectional TEM images of (b) a *c*-grain and (c) an *a*-grain. High-resolution TEM images of the lattices and FFT patterns from different regions of the films are inserted in panels b and c.

Figure 7 showed pseudostatic P-E hysteresis loops of the CBNO films measured at 1 kHz and different maximum electric fields $(E_{\rm max})$, demonstrating the process of pseudostatic saturation of the polarization. ⁴⁷ A "saturated"/maximum polarization $(P_{\rm s})$ of $\sim 60~\mu{\rm C/cm^2}$, a remnant polarization $(P_{\rm r})$ of $\sim 14~\mu{\rm C/cm^2}$, and a coercive field $(E_{\rm c})$ of $\sim 330~{\rm kV/cm}$ were obtained for the CBNO films $(@E_{\rm max}=2600~{\rm kV/cm})$. The improvements in electrical polarizations $P_{\rm S}$ and $P_{\rm r}$ are due to different reasons. The improved iP_S is indeed an improved electrical displacement $(P_{\rm S}=D_{\rm S}=P+\varepsilon_{\rm r}E,$ where P is the self-polarization under a field E and $P\approx P_{\rm r}$ for ferroelectrics), which can be attributed to the strain-enhanced dielectric constant $\varepsilon_{\rm r}$

and hence reflects an improved dielectric property. On the other hand, the improved $P_{\rm r}$ shows an enhanced ferroelectricity, which can be explained by the increased amount of a-grains in our strain-engineered CBNO films. Compared with the results reported by Y. Ahn et al. for their highly a-axis textured CBNO films, 29 the polarization responses of our CBNO films were significantly improved by applying higher electric fields. At $E=2600~{\rm kV/cm}$, the observed polarization values ($P_{\rm r}\approx 14~\mu{\rm C/cm}^2$ and $P_{\rm s}\approx 60~\mu{\rm C/cm}^2$) are the highest reported for CBNO materials, including both films and ceramics.

The good quality of our films results in a high breakdown electrical field, which is higher than 2600 kV/cm or 2.6 MV/

ACS Applied Materials & Interfaces

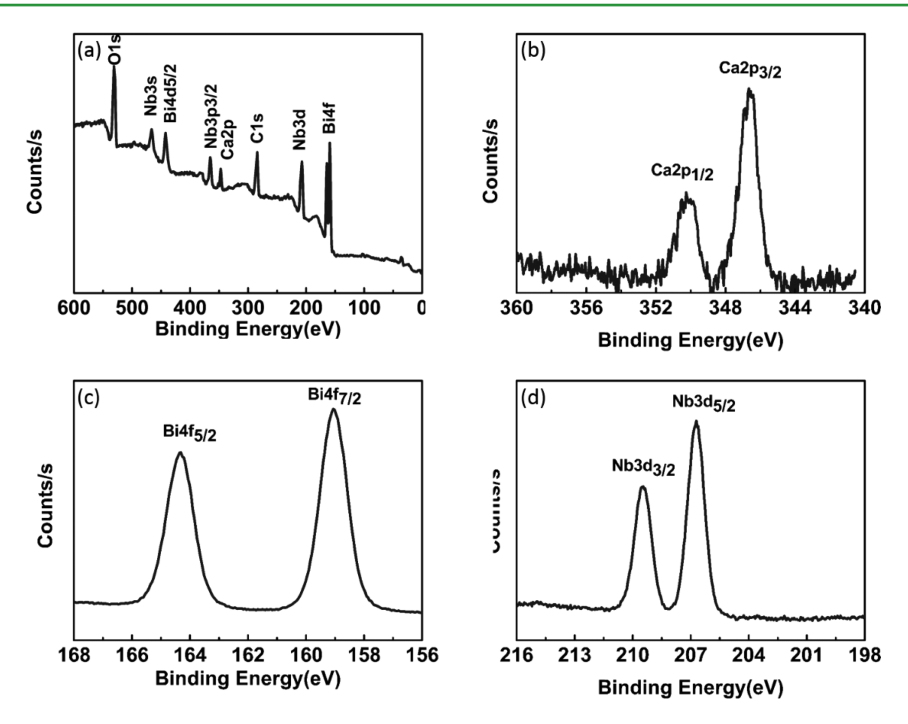


Figure 5. (a) XPS spectrum of the CBNO film in the energy range of 0–600 eV; panels b–d are the XPS spectra of Ca 2p core level, Bi 4f core level, Nb 3d core level, respectively.

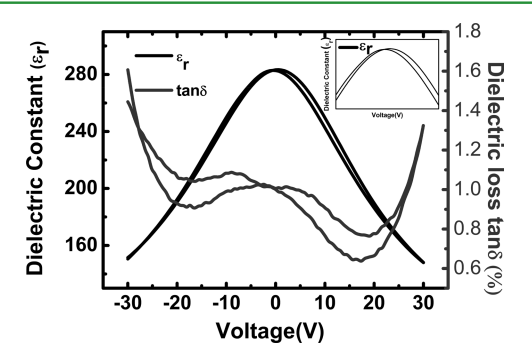
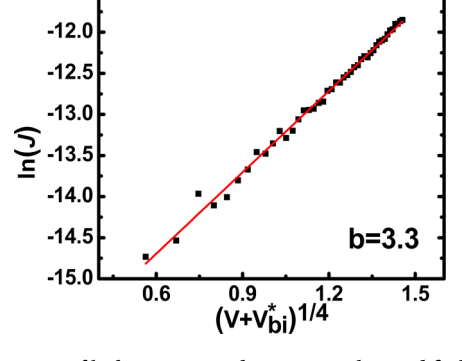


Figure 6. Relative dielectric constant (ε_r) and loss tangent $(tg\delta)$ of the CBNO film as a function of applied electric voltage. The part of the ε_r -V curve near zero field was zoomed in and inserted on the top.



-11.5

Figure 8. Fitting of leakage current densities via the modified Schottky contact model for J–V curves of the CBNO film.

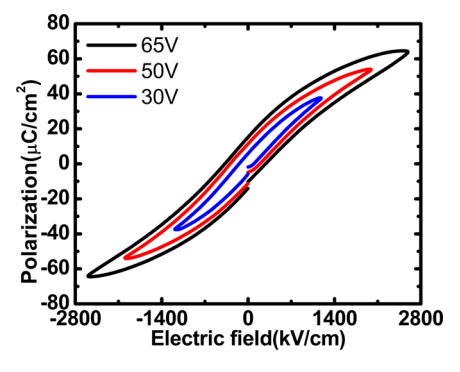


Figure 7. Ferroelectric hysteresis loops of the CBNO film measured at a maximum applied electric field of 1200, 2000, and 2600 kV/cm (@ 1 kHz).

cm, beyond which the P-E hysteresis loop showed a clear sign of conduction behavior. In addition, it is easy to notice the shrinking and tilting of the P-E loops. This type of P-E loops are commonly observed in CBNO materials $^{8,23-27}$ and can be attributed to the effect of a space charge layer. $^{47-49}$ Figure 8

shows a good fitting of the leakage current density-electric voltage curve (J-V curve) of the CBNO film to a modified Schottky contact model. ^{47,50} The space-charge density (N_{eff}) of the film can be estimated from the fitted J-V curve using the formula $(J) = b (V + V_{bi}^*)^{1/4}$, where b is the fitted slope and

$$b = \frac{q}{KT} \sqrt[4]{\frac{q^3}{8\pi^2 e_0^2 \epsilon_{dy}^2 \epsilon_r} N_{\text{eff}}} ^{47,50}$$
 Here V_{bi}^* is the built-in interface

potential related to the height of the interface energy barrier between the CBNO film and the electrode layer, and the value of V_{bi}^{k} is about 0.5 V. q is the electron charge, k is the Boltzmann constant, and T the temperature in Kelvin (T=298 K is used for room temperature). ε_{0} , ε_{dy} , and ε_{r} are the vacuum permittivity, dynamic, and static dielectric constants of the CBNO film, respectively. The static dielectric constant can be obtained from the $\varepsilon_{r}-V$ curves under zero bias (\sim 280). The value of dynamic dielectric constant ε_{dy} of the CBNO film is estimated to be in the range of $[4,30]^{.51}$. On the basis of the fitted value of b (see Figure 8) and measured/estimated dielectric constants, a space-charge density $N_{\rm eff}$ in the range of $[3.5 \times 10^{19} \ {\rm cm}^{-3}$, $2.0 \times 10^{20} \ {\rm cm}^{-3}$] was estimated for the

CBNO films. As Scott et al. reported in the literature, ⁴⁸ the P-E hysteresis loop of a ferroelectric film would shrink and tilt substantially with a space-charge concentration on the order of 10¹⁹ cm⁻³ or above. Our CBNO films fall into this special category of ferroelectric films, that is, space-charge dominated ferroelectric films.

4. CONCLUSION

In conclusion, strain engineered CaBi₂Nb₂O₉ thin films were deposited on MgO substrates via RF magnetron sputtering. The films exhibited a 2-fold increase in dielectric constant ($\varepsilon_{\rm r} \approx$ 283) as compared to previously reported results. This high dielectric constant can be attributed to the two effects from strain engineering, that is, an increased amount of a-grains, and an in-plane tensile stress. Moreover, the increase in dielectric constant comes with a low dielectric loss tangent ($tg\delta \leq 1.6\%$) and a high dielectric tunability (~47%), indicating a good potential of the CBNO films to be used as high-performance thin film dielectric capacitors, phase shifters and varactors. On the other hand, although the P-E hysteresis loops showed shrinking and tilting characteristics due to a high space-charge density, a substantial improvement in ferroelectric property (P_r $\approx 14 \ \mu\text{C/cm}^2$) was achieved in the CBNO films, due to an increased amount of electrically active grains. Meanwhile, the increase of maximum polarization, P_s , was mostly due to a large linear contribution from the high dielectric constant.

ASSOCIATED CONTENT

S Supporting Information

The Supporting Information is available free of charge on the ACS Publications website at DOI: 10.1021/acsami.6b00298.

Line scans of TEM images, EDS spectrum, piezoelectric force microscopy (PFM) image, illustration of compensation charge flowing caused by polarization switching, P−E hysteresis loop, current loop, and statements of the ferroelectricity (PDF)

AUTHOR INFORMATION

Corresponding Authors

*E-mail: ouyangjun@sdu.edu.cn.

*E-mail: wangcm@sdu.edu.cn.

Notes

The authors declare no competing financial interest.

ACKNOWLEDGMENTS

The authors acknowledge the financial support of the NSFC of China (Project Grant No. 91122024 and No. 50902087), the NSFC of Shandong Province of China (Project Grant No. ZR2012EMQ005 and ZR2014EMM012) and Program for New Century Excellent Talents in University (State Education Ministry), Nano Projects of Soochow City (Grant No. ZXG201445), the Fundamental Research Funds of Shandong University (Grant Nos. 2015JC034, 2015YQ009 and 2016JC036), and a foundation under the Grant no.2015JMRH0103. J.O. would also like to thank the "Qi-Lu Young Scholar Fund" of Shandong University and the support from the Material Measurement Laboratory of NIST, Gaithersburg, MD (USA).

REFERENCES

(1) Aurivillius, B. Mixed Bismuth Oxides with Layer Lattices. J. Ark Kem. 1949, 1, 463-512.

- (2) Lee, H. N.; Hesse, D.; Zakharov, N.; GÕsele, U. Ferroelectric Bi_{3,25}La_{0,75}Ti₃O₁₂ Films of Uniform a-axis Orientation on Silicon Substrates. Science 2002, 296, 2006-2009.
- (3) Yan, H. X.; Li, C. E.; Zhou, J. G.; Zhu, W. M. Structures and Properties of Bismuth Layer-structured Piezoelectric Ceramics with High T_c. J. Inorg. Mater. 2000, 15, 209-220.
- (4) Yan, H. X.; Zhang, H. T.; Reece, M. J.; Dong, X. L. Thermal Depoling of High Curie Point Aurivillius Phase Ferroelectric Ceramics. Appl. Phys. Lett. 2005, 87, 082911.
- (5) Zhang, S. J.; Yu, F. P. Piezoelectric Materials for High Temperature Sensors. J. Am. Ceram. Soc. 2011, 94, 3153-3170.
- (6) Scott, J. F.; Paz de Araujo, C. A. Ferroelectric Memories. Science 1989, 246, 1400-1405.
- (7) Ramesh, R.; Schlom, D. G. Orienting Ferroelectric Films. Science 2002, 296, 1975-1976.
- (8) Yan, H. X.; Zhang, H. T.; Ubic, R.; Reece, M. J.; Liu, J.; Shen, Z. J.; Zhang, Z. A. A Lead-Free High-Curio-Point Ferroelectric Ceramic, CaBi₂Nb₂O₉. Adv. Mater. 2005, 17, 1261–1265.
- (9) Chen, H. B.; Fu, F.; Zhai, J. W. Fabrication and Piezoelectric Property of Highly Textured CaBi₂Nb₂O₉ Ceramics by Tape Casting. Jpn. J. Appl. Phys. 2011, 50, 050207.
- (10) Chen, H. B.; Shen, B.; Xu, J. B.; Kong, L. B.; Zhai, J. W. Correlation between Grain Sizes and Electrical Properties of CaBi₂Nb₂O₉ Piezoelectric Ceramics. J. Am. Ceram. Soc. 2012, 95, 3514-3518.
- (11) Tian, X. X.; Qu, S. B.; Du, H. L.; Li, Y.; Xu, Z. Effects of (LiCe) Co-substitution on the Structural and Electrical Properties of CaBi₂Nb₂O₉ Ceramics. Chin. Phys. B 2012, 21, 037701.
- (12) Wang, C. M.; Wang, J. F.; Zhang, S. J.; Shrout, T. R. Piezoelectric and Electromechanical Properties of Ultrahigh Temperature CaBi₂Nb₂O₉ Ceramics. Phys. Status Solidi RRL 2009, 3, 49-51.
- (13) Ismailzade, I. G. X-ray Diffraction Study of the Structure of New Layered Ferroelectrics. Izv. Akad. Nauk SSSR, Ser. Fiz. 1960, 24, 1196-1202.
- (14) Blake, S. M.; Falconer, M. J.; McCreedy, M.; Lightfoot, P. Cation Disorder in Ferroelectric Aurivillius Phases of the Type $Bi_2ANb_2O_9$ (A = Ba, Sr, Ca). J. Mater. Chem. 1997, 7, 1609–1613.
- (15) Chen, H. B.; Zhai, J. W. Enhancing Piezoelectric Performance of CaBi₂Nb₂O₉ Ceramics through Microstructure Control. J. Electron. Mater. 2012, 41, 2238-2242.
- (16) Peng, D. F.; Zou, H.; Xu, C. N.; Li, J.; Wang, X. S.; Yao, X. Photoluminescent and Dielectric Characterizations of Pr Doped CaBi₂Nb₂O₉ Multifunctional Ferroelectrics. Ferroelectrics 2013, 450, 113-120.
- (17) Zhang, X. D.; Yan, H. X.; Reece, M. J. Effect of A Site Substitution on the Properties of CaBi₂Nb₂O₉. J. Am. Ceram. Soc. 2008, 91, 2928-2932.
- (18) Chen, H. B.; Zhai, J. W.; Guo, X. X.; Cui, Z. H. Effects of A-Site Sm Substitution and Textured Structure on Electric Properties of CaBi₂Nb₂O₉-Based High-Curie Temperature Ceramics. Int. J. Appl. Ceram. Technol. 2013, 10, E151-158.
- (19) Zhang, H. T.; Yan, H. X.; Reece, M. J. Microstructure and Electrical Properties of Aurivillius Phase (CaBi₂Nb₂O₉)_{1 x} (Ba-Bi₂Nb₂O₉) x Solid Solution. J. Appl. Phys. 2010, 108, 014109.
- (20) Tian, X. X.; Qu, S. B.; Pei, Z. B.; Tian, C. H.; Xu, Z. Microstructure, Dielectric, and Piezoelectric Properties of Ce-Modified CaBi₂Nb₂O₉ Ceramics. Ferroelectrics 2010, 404, 127-133.
- (21) Bao, S. M.; Peng, Z. H.; Guang, W. Y.; Li, Q. C.; Zhang, W.; Xiao, D. Q.; Zhu, J. G.; et al. Effects of Mn and Pr Co-Doped on Microstructural and Electrical Properties of CaBi₂Nb₂O₉ Piezoceramics. Ferroelectrics 2014, 458, 200-207.
- (22) Desu, S. B.; Cho, H. S.; Joshi, P. C. Highly Oriented Ferroelectric CaBi₂Nb₂O₉ Thin Films Deposited on Si(100) by Pulsed Laser Deposition. Appl. Phys. Lett. 1997, 70, 1393-1395.
- (23) Cho, H. S.; Desu, S. B. Structural and Electrical Properties of Oriented Ferroelectric CaBi₂Nb₂O₉ Thin Films Deposited on Si (100) by Pulsed Laser Deposition. Phys. Status Solidi 1997, 161, 371-378.
- (24) SimÕes, A. Z.; Ries, A.; Riccardi, C. S.; Gonzalez, A. H. M.; Longo, E.; Varela, J. A. High Curie Point CaBi₂Nb₂O₉ Thin Films: A

- Potential Candidate for Lead-Free Thin Film Piezoelectrics. J. Appl. Phys. 2006, 100, 074110.
- (25) SimÕes, A. Z.; Riccardi, C. S.; Cavalcante, L. S.; Longo, E.; Varela, J. A.; Mizaikoff, B. Impact of Oxygen Atmosphere on Piezoelectric Properties of CaBi₂Nb₂O₉ Thin Films. *Acta Mater.* **2007**, 55, 4707–4712.
- (26) SimÕes, A. Z.; Ramirez, M. A.; Ries, A.; Wang, F.; Longo, E.; Varela, J. A. Microwave Synthesis of Calcium Bismuth Niobate Thin Films Obtained by the Polymeric Precursor Method. *Mater. Res. Bull.* **2006**, *41*, 1461–1467.
- (27) SimÕes, A. Z.; Ramirez, M. A.; Riccardi, C. S.; Gonzalez, A. H. M.; Longo, E.; Varela, J. A. Synthesis and Electrical Characterization of CaBi₂Nb₂O₉ Thin Films Deposited on Pt/Ti/SiO₂/Si Substrates by Polymeric Precursor Method. *Mater. Chem. Phys.* **2006**, *98*, 203–206.
- (28) Ahn, Y.; Seo, J. D.; Son, J. Y. Ferroelectric Domain Structures of Epitaxial CaBi₂Nb₂O₉ Thin Films on Single Crystalline Nb Doped (1 0 0) SrTiO₃ Substrates. *J. Cryst. Growth* **2015**, 422, 20–23.
- (29) Ahn, Y.; Son, J. Y. Improved Ferroelectric Property and Domain Structure of Highly *a*-Oriented Polycrystalline CaBi₂Nb₂O₉ Thin Film. *J. Cryst. Growth* **2015**, 432, 92–94.
- (30) Bhaskaran, M.; Sriram, S.; Rodriguez, B. J.; Devendra, G. C.; Latham, K.; McCulloch, D. G.; Mitchell, A. Lattice Guiding for Sputter Deposition of Single Domain (Sr_{0.6}Ba_{0.4})Nb₂O₆ Ferroelectric Thin Films. *CrystEngComm* **2012**, *14* (2), 359–361.
- (31) Vu, H. T.; Nguyen, M. D.; Houwman, E.; Boota, M.; Dekkers, M.; Vu, H. N.; Rijnders, G. Ferroelectric and Piezoelectric Responses of (110) and (001)-Oriented Epitaxial Pb(Zr_{0.5}2Ti_{0.48})O₃ Thin Films on All-oxide Layers Buffered Silicon. *Mater. Res. Bull.* **2015**, 72, 160–167.
- (32) Nagarajan, V.; Alpay, S. P.; Ganpule, C. S.; Nagaraj, B. K.; Aggarwal, S.; Williams, E. D.; Roytburd, A. L.; Ramesh, R. Role of Substrate on the Dielectric and Piezoelectric Behavior of Epitaxial Lead Magnesium Niobate-lead Titanate Relaxor Thin Films. *Appl. Phys. Lett.* **2000**, *77* (3), 438–440.
- (33) Slutsker, J.; Artemev, A.; Roytburd, A. L. Engineering of Elastic Domain Structures in a Constrained Layer. *Acta Mater.* **2004**, *52* (6), 1731–1742.
- (34) Watanabe, T.; Funakubo, H. Epitaxial Growth Map for Bi₄Ti₃O₁₂ Films: A Determining Factor for Crystal Orientation. *Jpn. J. Appl. Phys.* **2005**, *44* (3R), 1337–1343.
- (3\$) Jo, W.; Kim, K.; Noh, T. Leakage Current Behaviors of Epitaxial and Preferentially Oriented Bi₄Ti₃O₁₂ Thin Films Grown on La_{0.5}Sr_{0.5}CoO₃ Bottom Electrodes. *Appl. Phys. Lett.* **1995**, *66* (23), 3120–3122.
- (36) Watanabe, T.; Funakubo, H. Controlled Crystal Growth of Layered-perovskite Thin Films as An Approach to Study Their Basic Properties. *J. Appl. Phys.* **2006**, *100* (5), 051602.
- (37) Zhang, W.; Kang, L. M.; Yuan, M. L.; Yang, Q.; Ouyang, J. Effect of Bottom Electrode on the Microstructure and Electrical Properties of Sputtered BaTiO₃ Films on MgO Substrates. *J. Alloys Compd.* **2013**, 580, 363–368.
- (38) Gao, W. L. Growth and Properties of Relaxor Ferroelectric Calcium Barium Niobate Series Crystals. Ph. D. Thesis, Shandong University, Jinan, China, 2010.
- (39) Durand, M. A. The Coefficient of Thermal Expansion of Magnesium Oxide. J. Appl. Phys. 1936, 7, 297–298.
- (40) Canedy, C. L.; Li, H.; Alpay, S. P.; Salamanca-Riba, L.; Roytburd, A. L.; Ramesh, R. Dielectric Properties in Heteroepitaxial Ba_{0.6}Sr_{0.4}TiO₃ Thin Films: Effect of Internal Stresses and Dislocation-type Defects. *Appl. Phys. Lett.* **2000**, *77*, 1695–1697.
- (41) Li, H.; Roytburd, A. L.; Alpay, S. P.; Tran, T. D.; Salamanca-Riba, L.; Ramesh, R. Dependence of Dielectric Properties on Internal Stresses in Epitaxial Barium Strontium Titanate Thin Films. *Appl. Phys. Lett.* **2001**, *78*, 2354–2356.
- (42) Ohring, M. The Materials Science of Thin Films, 2nd ed.; Academic Press, 2002.
- (43) Zhu, H.; Sun, X.; Kang, L.; Hong, M.; Liu, M.; Yu, Z.; Ouyang, J. Charge Transport Behaviors in Epitaxial BiFeO₃ Thick Films

- Sputtered with Different Ar/O₂ Flow Ratio. Scr. Mater. **2016**, 115, 62–65.
- (44) Zhu, H.; Kang, L.; Sun, X.; Zhang, Y.; Yu, Z.; Ouyang, J.; Pan, W. Microstructural and Electrical Characteristics of Epitaxial BiFeO3 Thick Films Sputtered at Different Ar/O2 Flow Ratios. *CrystEngComm* **2016**, *18*, 4604.
- (45) Tsai, H. M.; Lin, P.; Tseng, T. Y. Effect of Bismuth Content on the Properties of $Sr_{0.8}Bi_xTa_{1.2}Nb_{0.9}O_{9+y}$. J. Appl. Phys. **1999**, 85 (2), 1095–1100.
- (46) Li, A.; Wu, D.; Ling, H.; Yu, T.; Wang, M.; Yin, X.; Liu, Z.; Ming, N. Effects of Processing on the Characteristics of $SrBi_2Ta_2O_9$ Films Prepared by Metalorganic Decomposition. *J. Appl. Phys.* **2000**, 88, 1035–1041.
- (47) Zhang, W.; Gao, Y. Q.; Kang, L. M.; Yuan, M. L.; Yang, Q.; Cheng, H. B.; Pan, W.; Ouyang, J. Space-charge Dominated Epitaxial BaTiO₃ Heterostructures. *Acta Mater.* **2015**, *85*, 207–215.
- (48) Zubko, P.; Jung, D. J.; Scott, J. F. Space Charge Effects in Ferroelectric Thin Films. J. Appl. Phys. 2006, 100, 114112.
- (49) Tagantsev, A. K.; Gerra, G. Interface-induced Phenomena in Polarization Response of Ferroelectric Thin Films. *J. Appl. Phys.* **2006**, *100*, 051607.
- (50) Pintilie, L.; Alexe, M. Metal-ferroelectric-metal Heterostructures with Schottky Contacts. I. Influence of the Ferroelectric Properties. *J. Appl. Phys.* **2005**, 98, 124103.
- (51) Das, R. R.; Bhattacharya, P.; Katiyar, R. S.; Bhalla, A. S. Leakage Current Behavior of SrBi₂Ta₂O₉ Ferroelectric Thin Films on Different Bottom Electrodes[J]. *J. Appl. Phys.* **2002**, 92 (10), 6160–6164. The dynamic dielectric constant $\varepsilon_{\rm dy}$ of SrBi₂Ta₂O₉ (SBT) thin film were measured to be 6.3 and 17 in two different experiment set-up. Based on the structure similarity between SBT and CBNO films (both are bismuth-layer structured ferroelectrics), as well as similar static dielectric constants $\varepsilon_{\rm r}$ (272, 137 for SBT and 280 for CBNO), we estimate that the dynamic dielectric constant of CBNO film is in the range of [4,30].